Macromolecules

Article

pubs.acs.org/Macromolecules

Quantitative Viscoelastic Mapping of Polyolefin Blends with Contact Resonance Atomic Force Microscopy

Dalia G. Yablon,*[,†] Anil Gannepalli,[‡] Roger Proksch,[‡] Jason Killgore,[§] Donna C. Hurley,[§] Jean Grabowski,[†] and Andy H. Tsou[†]

[†]Corporate Strategic Research, ExxonMobil Research and Engineering, Annandale, New Jersey 08801, United States

[‡]Asylum Research, Santa Barbara, California 93117, United States

[§]Materials Reliability Division, National Institute of Standards and Technology, Boulder, Colorado 80305, United States

ABSTRACT: The storage modulus (E') and loss modulus (E'') of polyolefin blends have been mapped on the nanoscale with contact resonance atomic force microscopy (CR-FM), a dynamic contact mode of atomic force microscopy (AFM). Modulus values measured on various components within a blend of polyethylene, polypropylene, and polystyrene compared favorably with expected moduli of individual pure components at the contact resonance frequency that were calculated from bulk dynamic mechanical analysis (DMA) measurement results. Absolute storage modulus values were in good agreement with DMA results, while the loss modulus values obtained from CR-FM were consistently lower than those acquired from DMA. Application of CR-FM to an elastomer-containing blend resulted in moduli map artifacts due to the elastomer's high adhesion and low storage modulus, illustrating its limitation in quantifying viscoelastic properties of soft elastomers. In spite of this current limitation, the results presented in this paper demonstrate the potential of contact resonance methods for quantifying nanoscale viscoelastic properties of certain thermoplastic polymers.

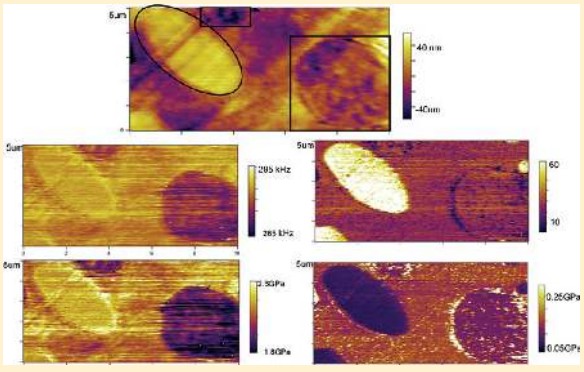

INTRODUCTION

Since its invention in 1986,[1] atomic force microscopy (AFM) has become a powerful technique for imaging materials on the nanoscale. A variety of AFM-based methods have been developed that generate contrast from various material properties including electrical, magnetic, morphological, and mechanical parameters. AFM's ability to provide image contrast based on mechanical properties is a distinctive feature of this microscopy. However, extracting quantitative information on a material's mechanical properties remains significantly more challenging than acquiring simple qualitative contrast and is the subject of much research activity.[2−4]

The nanomechanical contrast provided by AFM allowed it to quickly become the method of choice in examining polymers. In general, polymers and polymer blends have little or no contrast in electron microscopy without metal oxide staining.[5] In addition, transmission electron microscopy requires cryomicrotomy to provide thin (∼100 nm) sections for effective imaging. On the other hand, AFM simply requires a smooth surface (usually obtained with cryo-facing) for direct imaging. Additionally, AFM contrast originating from a sample's mechanical properties used for AFM contrast in polymer systems are themselves the properties of interest, as many products are formulated to exhibit particular mechanical properties. As polymer manufacturers continue to invent and deliver polymer blends and composites with submicrometer dispersions and domains prepared both *in situ* during the polymer synthesis and *ex situ* by postreactor compounding, the ability to quantify mechanical properties of polymers on the nanoscale is becoming increasingly important.

Several available AFM-based methods provide contrast based on mechanical properties on the nanoscale, with tapping mode (or amplitude modulation mode) phase imaging[6,7] the most popular and routinely used method for polymer characterization. In tapping mode, the phase of the cantilever oscillation shifts due to interactions with the sample. In phase imaging this phase shift is recorded as the cantilever probes different regions of the sample. There are numerous application examples using phase imaging to characterize polymeric materials including recent examples characterizing commercially important polymers,[8] elastomer and thermoplastic blends,[9,10] polymer crystallization,[11] block copolymers[12−14] and polymer nanocomposites.[15,16] However, the use of phase imaging to acquire quantitative materials contrast for practical imaging applications remains challenging[17] with recent progress in interpretation of phase signal through conservative and dissipative cantilever response[2,18,19] and loss tangent of the surface.[20,21]

Received: December 29, 2011
Revised: March 16, 2012
Published: May 9, 2012

   dx.doi.org/10.1021/ma2028038 | *Macromolecules* 2012, 45, 4363−4370

Other AFM-based methods that have been applied for quantitative nanomechanical characterization include force modulation,[22] peak force quantitative nanomechanical mapping (QNM),[23] intermodulation spectroscopy,[24] pulsed force mode,[25] and force volume imaging.[26] Contact resonance (CR) techniques are dynamic contact modes of AFM that were originally developed to measure elastic properties of stiff materials,[27−30] including polymer nanotubes.[31] In CR techniques, vibrational resonances of the AFM cantilever are excited while the tip is in contact with the sample. CR techniques can be implemented in various ways including actuation of either the sample (atomic force acoustic microscopy, AFAM)[27] or the cantilever base (ultrasonic AFM, UAFM).[28] Contact resonance force microscopy (CR-FM) is an imaging approach in which the CR frequency is rapidly tracked during scanning, and the measured frequencies are used to determine a map of elastic modulus.[30] A broader range of frequencies could be explored by measuring the CR frequency of many different eigenmodes of a given cantilever[32] or by using a series of cantilevers with varying natural frequencies. CR-FM can probe at different measurement depths, depending on the load set by the user. Recently, CR-FM has been extended to measure viscoelastic properties of materials.[33−36] In viscoelastic CR-FM, the frequency and quality factor (a measure of the peak's sharpness) of the contact resonance spectrum are used to derive storage and loss moduli of the material under investigation.[19,24]

In this study, we measure the storage and loss moduli of individual components in two blends with viscoelastic CR-FM. Specifically, we examine a ternary blend composed of polypropylene, polyethylene, and polystyrene and a binary blend of polypropylene with a brominated isobutylene copolymer-based elastomer. Values for the storage and loss moduli for the components within the ternary blend obtained by CR-FM agree with the values obtained on bulk samples of the individual components by macroscopic dynamic mechanical analysis (DMA) methods. DMA data were converted to high frequency for comparison to the CR-FM results via time temperature superposition. Results for the elastomer-containing blend do not match our expectations, demonstrating a current limitation of the CR-FM technique and specifically the associated models used to derive the various viscoelastic parameters.

EXPERIMENTAL SECTION

Materials. Materials in the polymer blends were thermoplastics of isotactic polypropylene [PP] (ExxonMobil Chemical Co., Houston, TX), linear polyethylene [PE] (ExxonMobil Chemical Co.), and polystyrene [PS] (Polysciences, Warrington, PA) and a thermoset elastomer of brominated poly(isobutylene-*co*-*p*-methylstyrene) [BIMS] (ExxonMobil Chemical Co.). Blends of 3:1:1 (by mass) of PP/PE/PS and 4:1 (by mass) PP/BIMS were prepared in a Brabender mixer at 180 °C, 60 rpm, and 5 min of mixing (Brabender Instruments, South Hackensack, NJ). All samples were cryo-faced using a microtome (Ultracut 6, Leica Mikrosysteme GmbH, Vienna, Austria) at −120 °C with a glass and a diamond knife prior to AFM imaging.

Cantilevers had a nominal spring constant of 2 N/m (Olympus Corp., Tokyo, Japan) with a free cantilever resonance of ∼70 kHz and a corresponding CR first mode resonance occurring in a range of 260−300 kHz.

Methods. *Dynamic Mechanical Analysis.* Dynamic mechanical analysis (DMA) was conducted using a DMTA (dynamic mechanical tensile analyzer) instrument (Rheometric) at 0.1% strain and 1 Hz. The DMA measurements were conducted at 1 Hz, while the AFM contact resonance measurement occurs at tens to hundreds of kilohertz. Time−temperature superposition was applied to convert the DMTA temperature axis to a frequency axis in order to derive the dynamic mechanical properties of these plastics and elastomer as a function of frequency at room temperature. Time−temperature superposition is an empirical procedure based on the general hypothesis that there is an equivalence between time (or frequency) and temperature behavior in a polymer. The shift in the relaxation spectrum of a polymer by temperature corresponds to the shift of its relaxation spectrum by frequency via the shift factor which can be measured experimentally. So, the entire modulus−time behavior of a polymer material can thus be measured by applying time−temperature correspondence to experimental measurements of polymer relaxations carried out on experimentally accessible time scales. In this study described here, time−temperature superposition was used to calculate the moduli of the different materials at the high frequencies used in our measurements based on the low-frequency DMA measurements. Thus, the DMA storage and loss moduli values expected for high frequencies could be directly compared to the CR-FM values measured at the same frequencies. The variability in the DMA measurement with respect to sample preparation and handling typically lead to ∼10% measurement uncertainty, which has been reflected in the DMA values reported in Table 1. The time−temperature equivalence, or superposition, shift factors for amorphous polystyrene follow the Willams, Landel, and Ferry (WLF) equation, where the shift factors for semicrystalline polyethylene and polypropylene are described with an Arrhenius equation. Parameters for the WLF equation and for the Arrhenius equation to calculate the shift factors for PS, PE, and PP were obtained from the literature[37] with equations in ref 38.

Table 1. Ratios of Storage Modulus (E') and Loss Modulus (E'') for Bulk PP, PE, and PS Used in the Ternary Blend[a]

E'	PP:PS	PP:PE
DMA (250 kHz)	0.88 ± 0.088	1.18 ± 0.12
CR-DART (280 kHz)	0.94 ± 0.04	1.17 ± 0.07
CR-BE (280 kHz)	0.99	1.26
E''	PP:PS	PP:PE
DMA (250 kHz)	4.2 ± 0.42	2.1 ± 0.21
CR-DART (280 kHz)	1.76 ± 0.62	1.20 ± 0.16
CR-BE (280 kHz)	3.49	1.45

[a]Ratios are compared for the macroscopic bulk DMA values calculated at 250 kHz via time−temperature superposition, contact resonance−DART AFM measurements, and contact resonance−BE AFM measurements.

The error associated with this shifting is unknown. However, the shifting of the PE and PP to the appropriate frequency range occurred during a transition of both of these materials where the derivative is large, whereas the shifting of the PS took place in a flat part of the modulus vs temperature curve. As a result, we can surmise that there would be greater uncertainty in the shifted values of PE and PP with respect to PS but have no way to quantify it at this time.

AFM and Contact Resonance. All AFM measurements were conducted with a MFP-3D AFM (Asylum Research, Santa Barbara, CA) equipped with a sample actuator (Contact Resonance Module, Asylum Research). All cryo-faced samples were epoxied directly onto the sample transducer to ensure good coupling between the sample and transducer. Contact resonance imaging was conducted by actuating the sample (AFAM) and operating in either dual ac resonance tracking (DART) mode[39] where the tip is raster scanned across the surface or band excitation (BE) mode where the tip makes point measurements on the surface.[40] Contact resonance experiments were typically conducted at a loading force of 40 nN. Assuming Hertzian contact mechanics and homogeneous material, we estimate that our contact resonance experiments on the thermoplastic materials result in a stress field that is most sensitive to material down to ∼30

dx.doi.org/10.1021/ma2028038 | *Macromolecules* 2012, 45, 4363−4370

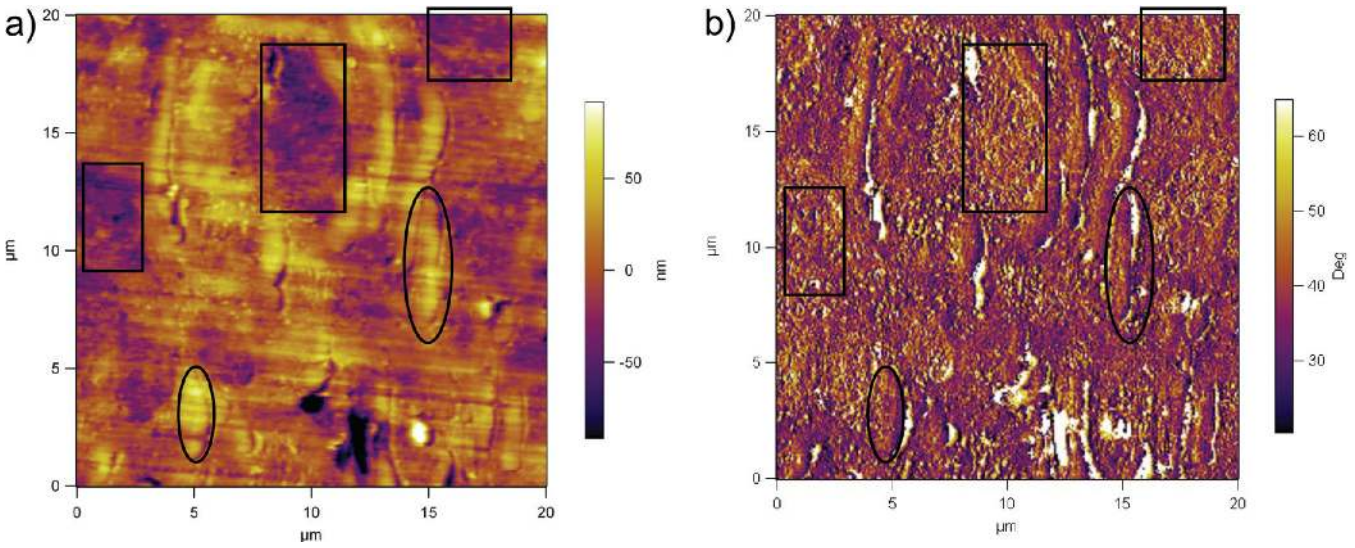

Figure 1. (a) Topography and (b) phase image of a 20 μm × 20 μm area of a ternary blend of 3:1:1 PP:PE:PS. Some domains of PS are circled, and some domains of PE are enclosed in a rectangle.

nm below the surface, which should be well below any near-surface effects that usually occur only in the first couple of nanometers near the surface.[41−43] For the BIMS material, the contact resonance experiments are most sensitive to material even further below the surface, to at least 100 nm below the surface.

DART mode tracks and images the contact resonance by monitoring the amplitude and phase response of the cantilever vibration at two frequencies near the contact resonance. In BE mode, the tip−sample contact is excited in a continuous band about the contact resonance. In both DART and BE mode, tip−sample contact is modeled as a damped simple harmonic oscillator (DSHO), and the amplitude and phase measurements near the contact resonance can be used for calculating the frequency and quality factor (Q factor) that are used to determine the storage and loss moduli, as described below.[35] In the implementation used here, BE is slower than the DART due to some specific hardware limitations associated with handling the large amount of data collected in BE mode. In DART, measurements at only two frequencies about the contact resonance are used to estimate the DSHO parameters, whereas in BE all the measurements in the continuous band (many more than two frequencies) are used to estimate the DSHO parameters. In this regard BE is much more data and measurement intensive when compared with DART. Once the DSHO parameters have been identified, the procedure to analyze and extract the mechanical properties is exactly the same.

Both DART[25] and BE modes yield two calculated images: one for the contact resonance frequency f and one for the quality factor Q of the contact resonance at each image pixel. The quality factor is a measure of the peak's sharpness given by $Q = f/\Delta f$, where Δf is the peak's full width at half-maximum (fwhm). These parameters can be used to obtain viscoelastic material properties (E', E'') as outlined below and discussed in more detail elsewhere.[33,34,44] Briefly, the experimental f and Q values are first related to the tip−sample contact stiffness and damping parameters with use of the Euler−Bernoulli model for the dynamic motion of the cantilever beam. The effect of the specimen's combined viscoelastic properties is included by modeling the tip−sample interaction as an elastic spring in parallel with a viscous dashpot. Application of Euler−Bernoulli beam theory leads to a characteristic equation that relates the normalized tip−sample contact stiffness α and damping coefficient β to the experimental f and Q.

Contact mechanics are then used to determine the viscoelastic properties at each image pixel from the values of α, β, and the contact resonance frequency f. An internal calibration approach was taken to determine absolute property values. In each image, the averages of α, β, and f for the continuous polypropylene (PP) phase were taken as the calibration values α_{cal}, β_{cal}, and f_{cal}, respectively. These were subsequently assumed to correspond to $E'_{cal} = E'_{PP} = 2.5$ GPa and $E''_{cal} = E''_{PP} = 126$ MPa, calculated at 250 kHz from DMA values. Assuming sphere-plane Hertzian contact, the reduced storage modulus E'^{R} and reduced loss modulus E''^{R} are obtained from

$$E'^{R} = E'^{R}_{cal}(\alpha/\alpha_{cal})^{3/2} \quad (1)$$

and

$$E''^{R} = E''^{R}_{cal}(f\beta/f_{cal}\beta_{cal})^{3/2} \quad (2)$$

Finally, assuming that Poisson's ratio ν is similar for the unknown and calibration materials, E' and E'' for each image pixel are extracted from the reduced complex modulus:

$$E^{*R} = E'^{R} + iE''^{R} = \left[\frac{1-\nu^2}{E'+iE''} + \frac{1}{M_{tip}}\right]^{-1} \quad (3)$$

Here, the tip indentation modulus $E'_{tip}/(1-\nu^2_{tip})$ was assumed to be 165 GPa for ⟨100⟩ silicon. Negligible damping in the tip ($E''_{tip} = 0$) was also assumed. All algorithms and analysis to generate maps of storage and loss modulus were conducted in the Asylum Research SPM software.

The CR-DART values reported in Table 1 for the various components represent averages of six different images, where all the PP, PE, and PS domains within a given image were included. The values of measurement uncertainty represent one standard deviation in the measurements from the six images. The CR-BE values reported in Table 1 are the average from all the PP, PE, and PS domains from a single image.

RESULTS

Ternary Blend. Conventional AFM phase imaging in tapping mode (in the net-repulsive regime) was conducted on the PP/PE/PS blend with resulting topographic and phase images shown in Figures 1a and 1b, respectively. The 20 μm × 20 μm image in Figure 1a reveals a PP matrix containing several PE and PS domains. The PE domains are enclosed in rectangles and can be distinguished by their slightly rougher surface and lower height (dark contrast) in the topographic image. The PE domain shapes are fairly round or slightly elliptical. The PS domains in Figures 1a and 1b are encircled in ovals and are distinguished by their fairly smooth surface, combined with the formation of narrower and elongated domains. The difference

dx.doi.org/10.1021/ma2028038 | Macromolecules 2012, 45, 4363−4370

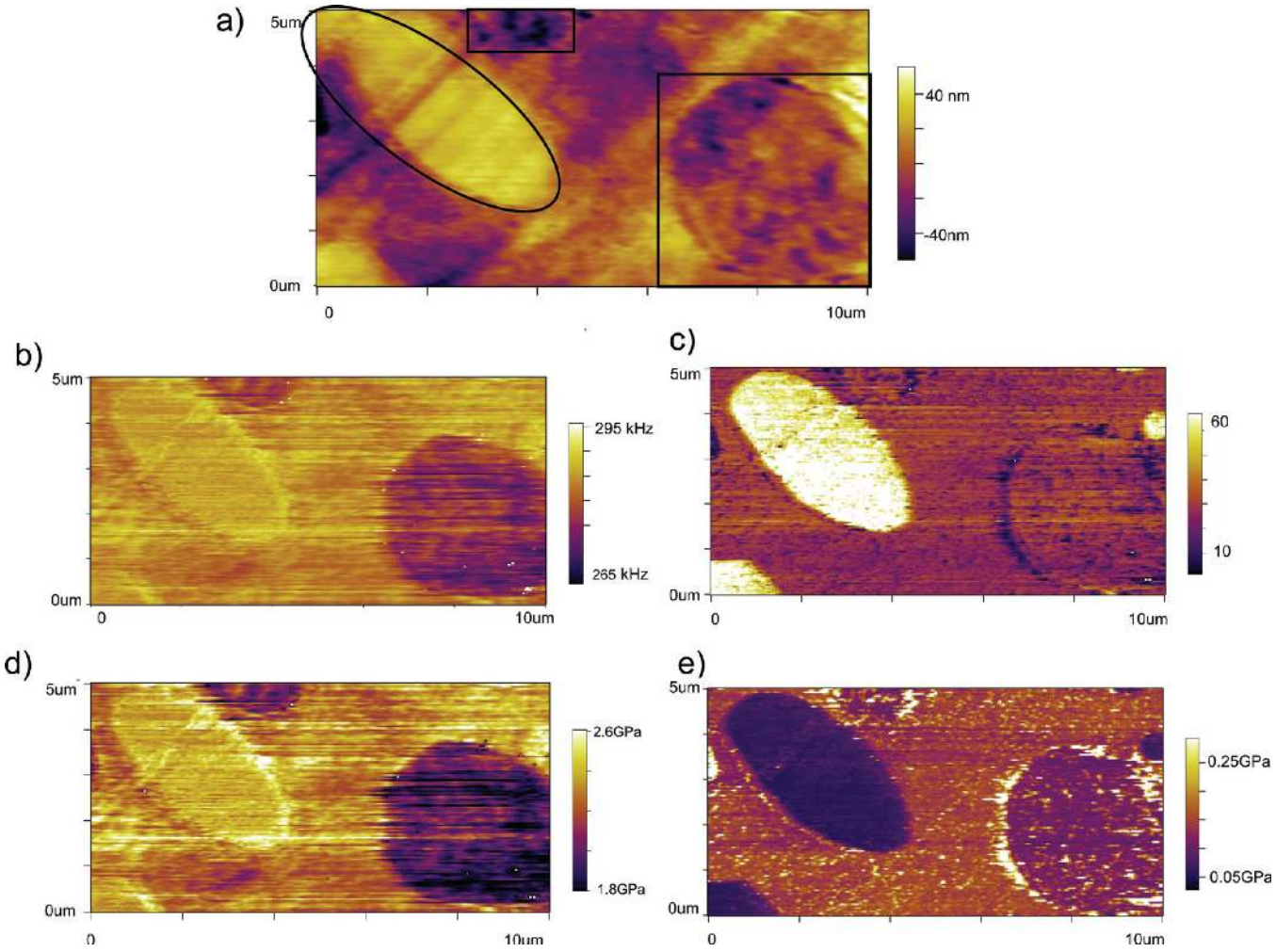

Figure 2. Images acquired in contact resonance-DART mode of a 10 μm × 5 μm area of the PP/PE/PS blend showing (a) topography, (b) contact resonance frequency, (c) quality factor, (d) calculated storage modulus, and (e) calculated loss modulus. The domains of PS are encircled, and domains of PE are enclosed in rectangles in (a).

between the domain shapes of PE and PS has to do with the mismatch between the viscosity of PE and PS dispersions and the viscosity of the PP matrix during mixing. The striations running across the topographical image are an artifact from the cryomicrotome process.

No significant phase contrast between the different materials is found in the phase image (Figure 1b). Similar to Figure 1a, some of the PS domains are encircled and some of the PE domains are enclosed in a rectangle, with the locations of these domains determined from the topographic image (Figure 1a). Bright white areas can be seen at the edges of some of the domains in the phase image. These white bands are the results of edge artifacts and are not related to the inherent material properties. The storage and loss moduli of these materials relative to PP (presented as ratios with PP), as calculated from time−temperature superposition at 250 kHz, are shown in Table 1. The values of loss moduli E'' of PE and PS are significantly different from that of PP, while their storage moduli $E'$are similar to that of PP. Despite this significant difference in loss modulus between all three materials, the phase signal shows little or no contrast. Although the interpretation of phase contrast is very challenging, as mentioned above, the lack of phase contrast among these materials is attributed to the loss tangents of PP, PE, and PS all being very small (<0.1). With such small loss tangents other uncertainties become significant. These include thermal noise of the cantilever, uncertainties in the exact determination of the resonance frequency, and unknown sample adhesive and attractive forces.

Contact resonance-DART results for this ternary blend are discussed below, with qualitative results described first followed by a quantitative comparison of all the data with DMA values at the relevant frequencies in the Discussion section. CR-DART on the same ternary blend from Figure 1 but from a different region are shown in a 10 μm × 5 μm image in Figure 2 and includes (a) topography, (b) CR frequency map, and (c) quality factor map, as well as the calculated quantitative maps of (d) storage modulus and (e) loss modulus obtained by the methods described above. As before, a PS domain has been encircled and the two PE domains are enclosed by a rectangle in the topography image in Figure 2a. The interface between the two materials has been affected by the cryotoming sample preparation and generally shows a delamination between two different materials that is not reflective of mechanical properties. The frequency map (Figure 2b) in this image shows little contrast between the PP and PS domains, but a lower CR frequency for the PE domains (~272 kHz) as compared to the other two (~282 kHz). The quality factor

dx.doi.org/10.1021/ma2028038 | *Macromolecules* 2012, 45, 4363−4370

map (Figure 2c) shows significant contrast between the PS domain ($Q \approx 66$) and the other two domains, which appear with similar contrast ($Q \approx 26$). The storage modulus map in Figure 2d shows little contrast between the PS and PP domains; in fact, the storage modulus ratio of $E'(\mathrm{PP})/E'(\mathrm{PS}) = 0.97$ for the particular image in Figure 2d. The PE domain, on the other hand, shows significantly lower storage modulus contrast compared with the PP and PS domains. We calculate a storage modulus ratio in Figure 2d of $E'(\mathrm{PP})/E'(\mathrm{PE}) = 1.17$. Assuming a storage modulus of 2.5 GPa for PP, as described in experimental methodology above, this results in $E'(\mathrm{PS}) = 2.4$ GPa and $E'(\mathrm{PE}) = 2.14$ GPa.

The loss modulus map in Figure 2e shows stronger contrast between the three materials. In the loss modulus map, the PS domains appear to be significantly darker than either the PE or PP domains, indicating a lower loss modulus. The PE response is between the PS and PP, suggesting that the loss modulus rank of these three materials follows PP > PE > PS. Material property ratios calculated from this specific image in Figure 2e are $E''(\mathrm{PP})/E''(\mathrm{PS}) = 2.40$ and $E''(\mathrm{PP})/E''(\mathrm{PE}) = 1.39$. Assuming a loss modulus of 126 MPa for PP as described above, this results in an $E''(\mathrm{PS}) = 52.5$ MPa and an $E''(\mathrm{PE}) = 90.6$ MPa. White points in the loss modulus map indicate data that was discarded because the assumptions of the model underlying the DART calculations were violated.[35]

Contact resonance-BE results of the ternary blend are shown in the 9 μm × 4.5 μm images in Figure 3 with topography obtained in conventional tapping mode in (a) and storage and loss moduli maps in (b) and (c), respectively, calculated from CR images acquired in band excitation (BE) mode. In its implementation on our platform, the BE technique is significantly slower than the DART technique. With the experimental parameters used to acquire Figure 3, a 32 pixel × 32 pixel BE image would have taken approximately the same time to collect as that required for a 512 pixel × 512 pixel DART image. For this reason, the storage and loss moduli map were collected with significantly lower spatial resolution than the DART maps in Figure 2. Also, the topography image in Figure 3a was a high resolution (256 pixel × 256 pixel) image collected in conventional tapping mode since the 32 pixel × 32 pixel topography image collected in BE mode (not shown) failed to show any features of interest due to its lower spatial resolution. Aside from the acquisition speed, there are other significant differences between contact resonance data acquisition via DART and point-mapping methods such as BE that have been addressed elsewhere.[34]

The BE images show similar trends in material properties to those in the DART images. The topography image in Figure 3a can be used as a guide, with PS domains encircled and PE domains enclosed in rectangles. The storage modulus map in Figure 3b shows little contrast between the PP and PS but significant contrast between the PE and the PP and PS materials, resulting in a ratio of $E'(\mathrm{PP})/E'(\mathrm{PE}) = 1.26$. In the loss modulus map in Figure 3c, the PS shows strong contrast with respect to the PP while the PE shows weak contrast with respect to the PP, with quantitative ratios of $E''(\mathrm{PP})/E''(\mathrm{PS}) = 3.49$ and $E''(\mathrm{PP})/E''(\mathrm{PE}) = 1.44$.

PP/BIMS Blend. Although the ternary blend sample provides a suitable test of viscoelastic CR-FM methods on model materials, it represents a limited class of materials relevant to the chemical and polymer industries. Many commercial blends and composite materials include a rubber or elastomer phase to improve a balance of various properties

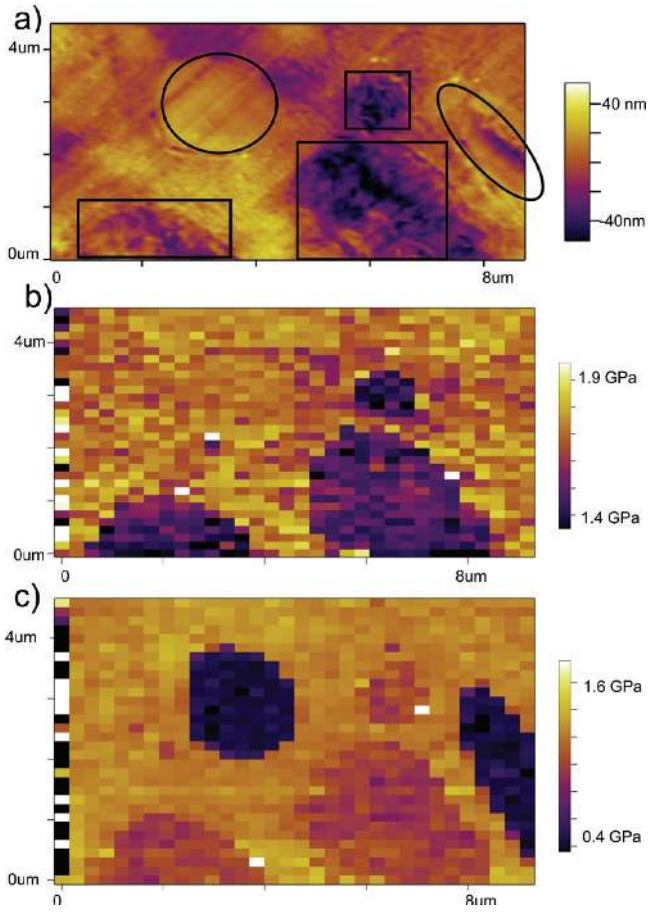

Figure 3. Contact resonance-BE images of a 10 μm × 5 μm area of the PP/PE/PS blend showing (a) topography, (b) storage modulus, and (c) loss modulus. The domain of PS is encircled, and domains of PE are enclosed in rectangles in (a).

such as stiffness, impact strength, and toughness. To that end, a blend of PP and BIMS was also explored with CR-FM in this study.

A contact resonance-DART image of a blend of PP and BIMS is shown in Figure 4. In the 5 μm × 5 μm height image in Figure 4a, a round (diameter ~1.5 μm) BIMS domain is observed in the middle of the PP matrix. As shown in Figure 4, the BIMS elastomer appears to be significantly depressed with respect to the PP matrix (several hundreds of nanometers) in the topography image, and the BIMS domain appears striated. Both of these features are artifacts induced by the scanning of a soft, highly damping elastomer sample in contact mode, (the mode of DART and some other CR-based techniques) where the tip may stick, deform, or drag the material, resulting in the observed striations. Band excitation mode, which is a pointwise technique, potentially addresses this limitation. However, in the current implementation, the band excitation method is very slow and would require several hours to acquire an image with reasonable resolution to test this hypothesis and was one of the reasons it was not conducted.

■ DISCUSSION

A quantitative comparison of the average ratio of storage and loss moduli obtained by viscoelastic CR-FM methods both in BE and DART collection modes with those calculated at 250 kHz from DMA data is presented in Table 1. The trends

dx.doi.org/10.1021/ma2028038 | Macromolecules 2012, 45, 4363−4370

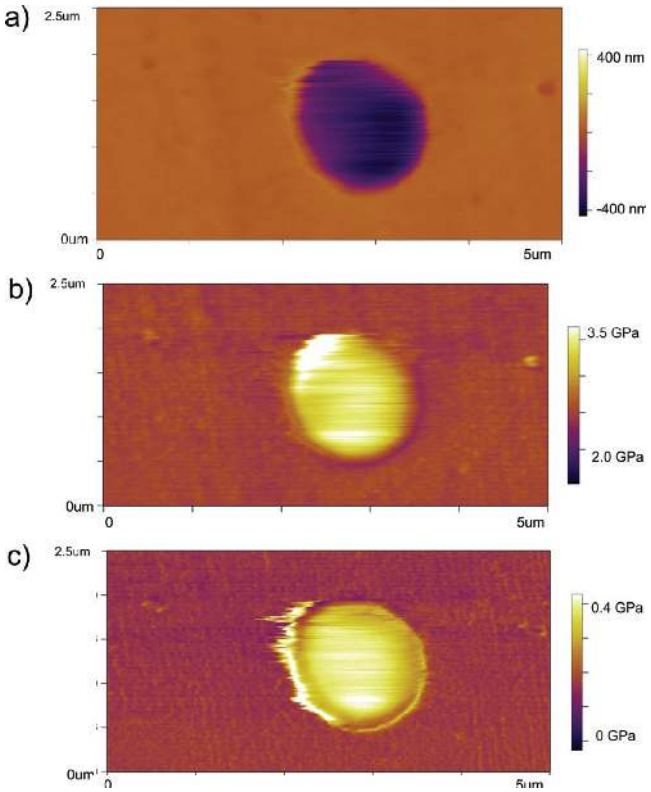

Figure 4. Contact resonance-DART image of a 5 μm × 2.5 μm area of a blend of PP/BIMS showing (a) topography, (b) storage modulus, and (c) loss modulus. The 1.5 μm diameter BIMS domain is clearly observed in the middle.

between the materials are consistent among all techniques, showing E'(PS) > E'(PP) > E'(PE) and E''(PP) > E''(PE) > E''(PS). According to the DMA results, the storage modulus E'(PS) is within 10% of E'(PP) value, while E'(PE) is within 20% of that for PP. The contact resonance images repeatedly showed a contrast between the storage modulus of PP and PE that compared favorably with that calculated from the DMA measurements. However, the contact resonance images did not always exhibit contrast in the storage modulus between PP and PS, perhaps indicative of the sensitivity limits of the technique. Images acquired in BE mode showed similar ratios to those from images acquired in DART mode for the relative storage moduli of all materials.

For loss moduli, where the differences are larger among the materials investigated, the contact resonance maps yielded ratios of PE and PS (relative to PP) that were generally lower than the DMA predictions. Within the contact resonance data, generally DART measurements yielded lower values than the values obtained from the BE measurements. We believe there are several possible reasons for the poorer agreement of the CR-FM and DMA loss modulus results compared to that of the storage modulus values. The first is related to the ability to accurately measure the quality factor Q. In the data analysis, the storage modulus value depends primarily on the contact resonance frequency, while the loss modulus depends more on both the frequency and the quality factor (sharpness) of the resonance spectrum.[44] The analysis approximates the tip−sample dynamics by a damped simple harmonic oscillator (DSHO) to calculate the resonance frequency and quality factor of the contact resonance spectrum. Since quality factor is more sensitive to changes in the shape of the contact resonance spectrum than resonant frequency, it may be more challenging to accurately determine the true quality factor than the resonance frequency. This applies in particular to DART mode, where Q is determined from the amplitude and phase measured at only two frequencies.[34] Because BE mode measures the entire contact resonance spectrum, its values for Q may be more robust. A second reason for the relatively poor agreement between CR-FM and DMA loss modulus values is the validity of assigning quality factor changes solely to changes in material damping. The quality factor is more dependent on factors such as amplitude of the contact resonance peak,[45] the surface adhesion damping, the topography variations, and the transfer function.[46] Finally, another issue may be the choice of CR eigenmode. The first (lowest-order) resonant eigenmode was used in these experiments, while in some cases, work with CR-FM for elastic modulus measurements has used higher-order modes to provide greater sensitivity or accuracy.[32]

The calculated storage and loss modulus maps of the PP/BIMS blend are shown in Figures 4b and 4c, respectively. The storage modulus map in Figure 4b indicates a higher storage modulus for the elastomer domain compared to the PP domain, consistent with a higher CR frequency on the elastomer over the PP (results not shown). This is clearly inconsistent with the DMA data that shows the elastomer having significantly lower storage modulus[47] than the PP. This is a good indication of the interpretational challenges faced by current CR-FM methods, especially for certain kinds of materials. The loss modulus map is however consistent with the DMA results, showing a higher loss modulus value for the BIMS compared to the PP. Attempts to obtain CR-FM with BE mode on the PP/BIMS sample failed to result in a completed image, for reasons discussed below.

Blends containing elastomers clearly present serious challenges to the current contact resonance methodology. First, contact mode scanning may not be suitable for soft elastomers, since the tip may stick to the elastomer and could damage the material from the high contact forces applied in this mode. Typically, tapping mode is a more effective and gentler imaging method for these types of soft materials and does not result in the striations in topography observed in contact mode (see Figure 4a). Second, the high damping of the BIMS elastomer presents problems for obtaining meaningful contact resonance spectra on this material via sample actuation beneath the sample. Contact resonance spectra on the PP and BIMS with the identical cantilever (Olympus AC 240, first mode free resonance at 70 kHz and first mode contact resonance at ∼280 kHz) and drive amplitude are shown in Figure 5 with the PP resonance curve in a dotted line/open points and the BIMS resonance curve in a solid line/filled points. The resonance curve on the BIMS is highly damped and represents a convolution of the response of the material and the piezo drive transfer function, which is the relationship between the drive voltage and the cantilever response. The signal-to-noise ratio (SNR) on the PP is higher than that on the BIMS elastomer, enabling the frequency and quality factor to be measured reasonably precisely on this material. The spectrum on the BIMS shows a very broad, heavily damped peak with a small SNR, indicating the challenges in making meaningful measurements of frequency and quality factor. In fact, the transfer function mentioned above may be dominating the measurement on the BIMS and thus lead to artifacts in the measurement, as has been observed in other systems.[46] It is for this reason that CR-FM in BE mode was unable to image this

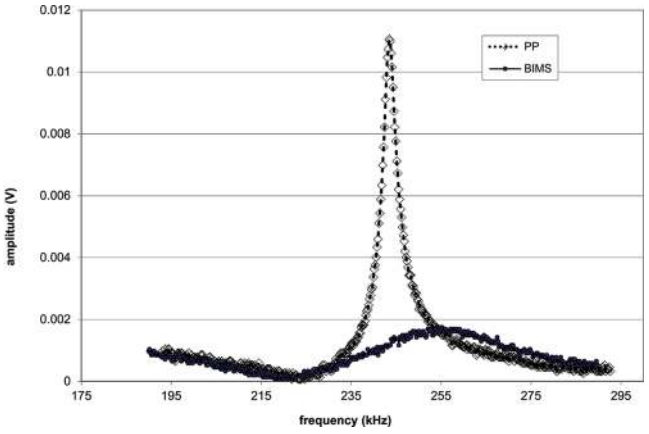

Figure 5. Sample contact resonance spectra for PP (dotted line, open points) and BIMS (solid line, solid points).

material due to the frequency tracking method used in BE that is more poorly equipped to handle a heavily damped response than DART. Note that in these two spectra the peak frequency on the BIMS (258 kHz) is higher than that on the PP (243 kHz), ultimately leading to the incorrect result observed in the storage modulus image in Figure 4b that the BIMS has a higher storage modulus than the PP.

There are additional challenges in applying CR to soft, highly damping elastomers such as BIMS. In particular, the current viscoelastic CR-FM analysis methodology used to derive material property values from contact resonance data is not entirely appropriate for elastomeric materials. First, the spring and dashpot combination used to model the tip−sample interaction only accommodates linear viscoelasticity, while elastomers may exhibit more complex behavior. In addition, the current viscoelastic CR-FM analysis methodology relies on a Hertzian model for the tip−sample interaction to extract the material properties of the sample from the tip−sample contact stiffness and damping.[33] The Hertzian model does not incorporate adhesion to describe the tip−sample contact. However, elastomers such as BIMS have significant adhesion, resulting in a larger effective tip−sample force and subsequent larger contact area for BIMS compared to PP that could result in the increased CR frequency on BIMS over PP as observed in Figure 4. Specifically, the contact area is determined through the relation $k = 2aE^*$, where k is the contact stiffness, a is the contact radius, and E^* is the reduced modulus. For a Hertzian contact, $a = (3RF_{total}/4E^*)^{1/3}$, where R is the tip radius of curvature and $F_{total}=F_{applied}$ is the total load. Then the ratio k_{BIMS}/k_{PP} between the contact stiffness on BIMS and PP is

$$\frac{k_{BIMS}}{k_{PP}} \approx \left(\frac{F_{total,BIMS}}{F_{total,PP}}\right)^{1/3}\left(\frac{E^*_{BIMS}}{E^*_{PP}}\right)^{2/3} \quad (4)$$

Adhesion is included in the Derjaguin−Müller−Toporov (DMT), $F_{total} = F_{applied} + F_{adhesion}$, where $F_{applied}$ is the set point force and $F_{adhesion}$ is the tip−sample pull-off force. In the context of this model, F_{total} on BIMS can be significantly higher than on PP even if $F_{applied}$ is equal for both materials because the adhesion on BIMS is much higher than PP. As can be observed from eq 4, this effect could overwhelm the smaller BIMS modulus, E^*_{BIMS}, resulting in and leading to a higher contact resonance frequency on BIMS compared to PP as observed in Figure 4.

Analyzing the CR-FM results with more advanced contact mechanics models such as the DMT model or Johnson−Kendall−Roberts (JKR) model[48] would perhaps be more appropriate. However, these models require corresponding adhesion force information, and the experimental challenge of scanning in contact mode on such a soft material would remain. Methods that combine slow, pointwise measurements with mechanics models incorporating adhesion or those that concurrently acquire adhesion with CR frequency and quality factor, and adhesion force,[49] may provide a path forward for contact resonance measurements on elastomeric materials like BIMS.

CONCLUSION

Contact resonance atomic force microscopy, a dynamic contact AFM mode, has been used to map the viscoelastic properties of polyolefin-containing blends. Contact resonance data were collected either in DART mode, where the cantilever's dynamic response is monitored at two frequencies, or in BE mode, where the entire frequency response is collected at every image pixel. Values for the storage and loss modulus of a ternary blend of polypropylene, polystyrene, and polyethylene obtained from CR-FM maps compared favorably with bulk DMA values calculated at high frequency via time−temperature superposition. There was more discrepancy between the CR-FM and DMA values for loss modulus, with the BE data comparing more favorably than the DART data. This variability was attributed primarily to the experimental challenges of accurately measuring the quality factor from the measurements. CR-FM mapping on a blend of PP/BIMS resulted in unrealistically high storage modulus values for the BIMS relative to the PP. Elastomers such as BIMS present significant challenges to contact resonance techniques in the current implementation, due to the AFM tip spreading the elastomer material in contact mode, a contact area that changes significantly between the elastomer and PP blends, and a model for contact mechanics analysis that does not account for adhesion. Nevertheless, these results demonstrate the potential of contact resonance methods for quantifying nanoscale viscoelastic properties of certain thermoplastic polymers.

AUTHOR INFORMATION

Corresponding Author

*E-mail: dalia.g.yablon@exxonmobil.com.

Notes

The authors declare no competing financial interest.

ACKNOWLEDGMENTS

The authors gratefully acknowledge Majia Amin (ExxonMobil Chemical Co.) for DMA data. This research was performed while JPK held an NRC Research Associateship Award at NIST. This work is a partial contribution of NIST, an agency of the US government. Mention of commercial equipment, instruments, or materials provides useful information, but does not imply recommendation or endorsement by NIST.

REFERENCES

(1) Binnig, G.; Quate, C. F.; Gerber, C. *Phys. Rev. Lett.* **1986**, *56*, 930−933.
(2) Gomez, C. J.; Garcia, R. *Ultramicroscopy* **2010**, *110*, 626−633.
(3) Martinez, N. F.; Garcia, R. *Nanotechnology* **2006**, *17*, S167−172.
(4) Cleveland, J. P.; Anczykowski, B.; Schmid, A. E.; Elings, V. B. *Appl. Phys. Lett.* **1998**, *72*, 2613−2615.

(5) Sawyer, L. C.; Grubb, D. T.; Meyers, G. F. *Polymer Microscopy*, 3rd ed.; Springer: Berlin, 2010.
(6) Zhong, Q.; Innis, D.; Kjoller, K.; Elings, V. *Surf. Sci. Lett.* **1993**, *290*, L688.
(7) Chernoff, D. A. In *Proceedings of Microscopy and Microanalysis*; Jones and Bagell: New York, 1995; p 888.
(8) Bar, G. K.; Meyers, G. F. *MRS Bull.* **2004**, *July*, 464−470.
(9) Achalla, P.; McCormick, J.; Hodge, T.; MOreland, C.; Esnault, P.; Karim, A.; Raghavan, D. *J. Polym. Sci., Part B* **2005**, *44*, 492−503.
(10) Gheno, S. M.; Passador, F. R.; Pessan, L. A. *J. Appl. Polym. Sci.* **2010**, *117*, 3211−3210.
(11) Hobbs, J. K.; Farrance, O. E.; Kailas, L. *Polymer* **2009**, *50*, 4281.
(12) Park, J. H.; Sun, Y.; Goldman, Y.; Composto, R. J. *Macromolecules* **2009**, *42*, 1017−1023.
(13) Djurisic, A. B.; Wang, H.; Chan, W. K.; Xie, M. H. *J. Scanning Probe Microsc.* **2006**, *1*, 21−31.
(14) Leclere, P.; Dubourg, F.; Kopp-Marsaudon, S.; Bredas, J. L.; Lazzaroni, R.; Aime, J. P. *Appl. Surf. Sci.* **2002**, *188*, 524−533.
(15) Wang, D.; Fujinami, S.; Nakajima, K.; Inukai, S.; Ueki, H.; Magario, A.; Noguchi, T.; Endo, M.; Nishi, T. *Polymer* **2010**, *51*, 2455−2459.
(16) Qu, M.; Deng, F.; Kalkhoran, S. M.; Gouldstone, A.; Robisson, A.; vanVliet, K. J. *Soft Matter* **2011**, *7*, 1066−1077.
(17) Attard, P. *J. Phys.: Condens. Matter* **2007**, *19*, 473201.
(18) Garcia, R.; Magerle, R.; Perez, R. *Nat. Mater.* **2007**, *6*, 405−411.
(19) Garcia, R.; Perez, R. *Surf. Sci. Rep.* **2002**, *47*, 197−301.
(20) Proksch, R.; Yablon, D. G. *Appl. Phys. Lett.* **2012**, *100*, 073106.
(21) Proksch, R.; Yablon, D. G.; Tsou, A. H. *Proc. ACS Rubber Div., 180th Tech. Meet.* **2011**, 24.
(22) Radmacher, M.; Tillman, R. W.; Gaub, H. E. *Biophys. J.* **1993**, *64*, 735−742.
(23) Young, T. J.; Monclus, M. A.; Burnett, T. L.; Broughton, W. R.; Ogin, S. L.; Smith, P. A. *Meas. Sci. Technol.* **2011**, *22*, 125703.
(24) Platz, D.; Tholen, E. A.; Pesen, D.; Haviland, D. B. *Appl. Phys. Lett.* **2008**, *92*, 153106.
(25) Rosa-Zeiser, A.; Weilandt, E.; Hild, S.; Marti, O. *Meas. Sci. Technol.* **1997**, *8*, 1333−1338.
(26) Wang, D.; Fujinami, S.; Nakajima, K.; Nishi, T. *Macromolecules* **2010**, *43*, 3169−3172.
(27) Rabe, U.; Arnold, W. *Appl. Phys. Lett.* **1994**, *64*, 1493−1495.
(28) Yamanaka, K.; Ogiso, H.; Kolosv, O. V. *Appl. Phys. Lett.* **1994**, *64*, 178.
(29) Hurley, D. C.; Shen, K.; Jennett, N. M.; Turner, J. A. *J. Appl. Phys.* **2003**, *94*, 2347−2354.
(30) Hurley, D. C. In *Applied Scanning Probe Methods*; Bhushan, B., Fuchs, H., Eds.; Springer-Verlag: Berlin, 2009; Vol. *XI*, pp 97−138.
(31) Cuenot, S.; Fretigny, C.; Demoustier-Champagne, S.; Nysten, B. *J. Appl. Phys.* **2003**, *93*, 5650.
(32) Killgore, J. P.; Hurley, D. C. *Nanotechnology* **2012**, *23*, 055702.
(33) Yuya, P. A.; Hurley, D. C.; Turner, J. A. *J. Appl. Phys.* **2008**, *104*, xxxx.
(34) Killgore, J. P.; Yablon, D. G.; Tsou, A. H.; Gannepalli, A.; Yuya, P. A.; Turner, J. A.; Proksch, R.; Hurley, D. C. *Langmuir* **2011**, *27*, 13983−13987.
(35) Gannepalli, A.; Yablon, D. G.; Tsou, A. H.; Proksch, R. *Nanotechnology* **2011**, *22*, 355705.
(36) Yablon, D. G.; Proksch, R.; Gannepalli, A.; Tsou, A. H. *Rubber Chem. Technol.* **2012**.
(37) van Krevelen, D. W. *Properties of Polymers*, 3rd ed.; Elsevier Science Publishers: Amsterdam, 1990; Chapter 13.
(38) a is shift factor, T_r is reference temperature (293 K). PS: $\log(a) = -14.5(T - T_g)/[50.4 + (T - T_g)]$. PE: $\log(a) = 23000(1/T - 1/T_r)$. PP: $\log(a) = 26450(1/T - 1/T_r)$.
(39) Rodriguez, B. J.; Callahan, C.; Kalinin, S.V.; Proksch, R. *Nanotechnology* **2007**, *18*, 475504.
(40) Jesse, S.; Kalinin, S. V.; Proksch, R.; Baddorf, A. P.; Rodriguez, B. J. *Nanotechnology* **2007**, *18*, 435503.
(41) Keddie, J. L.; Jones, R. A. L.; Cory, R. A. *EPL* **1994**, *27*, 59−64.
(42) Zhang, Y.-F.; Bai, S.-L.; Yang, D.-Y.; Zhang, Z.; Kao-Walter, S. *J. Polym. Sci., Part B* **2008**, *46*, xxxx.
(43) Torres, J. M.; Stafford, C. M.; Vogt, B. D. *ACS Nano* **2009**, *3*, 2677−2685.
(44) Yuya, P. A.; Hurley, D. C.; Turner, J. A. *J. Appl. Phys.* **2011**, *109*, 113528.
(45) Yamanaka, K.; Maruyama, Y.; Tsuji, T.; Nakamoto, K. *Appl. Phys. Lett.* **2001**, *78*, 1939−1941.
(46) Proksch, R.; Kalinin, S. V. *Nanotechnology* **2010**, *21*, 455705/1.
(47) Fu, M. *Rubber World* **1997**, 35−40.
(48) Johnson, K. L. *Contact Mechanics*; Cambridge University Press: Cambridge, UK, 1985.
(49) Killgore, J. P.; Hurley, D. C. *Appl. Phys. Lett.* **2012**, *100*, 053104.

NOTE ADDED AFTER ASAP PUBLICATION

This paper was published on the Web on May 9, 2012. Ref 20 has been revised, and corresponding author contact information has been added. The correct version was reposted on May 14, 2012.